# Synoptic and Mesoscale Aspects of the June 2013 Flooding in Uttarakhand, India

R. A. Houze, Jr. \*, \*, \*, \*, \*, \* K. L. Rasmussen +2, L. McMurdie \*, M. M. Chaplin \*, and A. Kumar #

\*Department of Atmospheric Sciences
University of Washington
Seattle, Washington USA

\$Pacific Northwest National Laboratory Richland, Washington USA

<sup>+</sup>Mesoscale and Microscale Meteorology Laboratory National Center for Atmospheric Research Boulder, Colorado

\*NASA Goddard Space Flight Center Earth System Science Interdisciplinary Center Greenbelt, Maryland

to be submitted

1

<sup>&</sup>lt;sup>1</sup> Corresponding author: Robert Houze, Department of Atmospheric Sciences, University of Washington, Box 351640, Seattle, WA 98195, Email address: houze@uw.edu

<sup>&</sup>lt;sup>2</sup> Current affiliation: Department of Atmospheric Science, Colorado State University

### **RUNNING HEAD**

Atmospheric Conditions Producing the Uttarakhand, India, Flood

### **KEYWORDS**

- Himalayas
- Flood
- India
- Uttarakhand

### **ABSTRACT**

Conditions producing disastrous flooding in Uttarakhand, India, in June 2013 differed from conditions producing other notorious floods in the Himalayan region in recent years. During the week preceding the Uttarakhand flood, deep convection moistened the mountainsides, making them vulnerable to flooding. However, the precipitation producing the flood was not associated with a deep convective event. Rather, an eastward propagating upper-level trough in the westerlies extended abnormally far southward, with the jet reaching the Himalayas. The south end of the trough merged with a monsoon low moving westward across India. The merged system produced a moist low-level jet oriented normal to the Himalayas that advected large amounts of water vapor into the Uttarakhand region. Orographic lifting of this moderately unstable moist air combined with wave-scale forcing to produce heavy continuous rain over the region for 2-3 days. The precipitation was largely stratiform in nature but contained embedded convection of moderate depth, especially along the foothills of the Himalayas, where the instability was being released. The Uttarakhand flood had characteristics in common with major 2013 floods in the Rocky Mountains in Colorado and Alberta.

### 1. Introduction

The northern Indian state of Uttarakhand lies in hills at the base of the steep south slopes of the central Himalayan escarpment (Figure 1). The northernmost part of the state consists of Himalayan peaks and glaciers. Deep valleys on the south-facing slopes are susceptible to landslides and flooding. Over a three-day period in June 2013, approximately 500-1000 mm of rain fell over Uttarakhand and its river valleys as well as neighboring Nepal. The extensive precipitation and runoff led to devastating floods and landslides throughout the region and resulted in much destruction and loss of life (over 4,000 villages were affected, and the death toll exceeded 5,000). The meteorological conditions leading to the Uttarakhand flood were unlike those of other major monsoon-season floods over and near the Himalayas in 2010-2012 (Houze et al. 2011, Rasmussen and Houze 2012, Rasmussen et al. 2015). Those floods were produced by deep and intense mesoscale convective systems (MCSs) forming in a moist airstream sandwiched between a strong low pressure system extending across northern India and anomalously high pressure over the Tibetan Plateau.

All but one of the 2010-2012 floods were slow-rising floods that lasted from a few days to over a month in the case of the 2010 Pakistan floods (Houze et al. 2011). However, one particular flood was different in that it was a flash flood rather than a slow-rising flood. Specifically, this flash flood was the notorious flood that occurred in Leh, India, in August 2010. The high-altitude city of Leh in the western portion of the Himalayas was struck by a strong, rapidly propagating MCS moving from the east off the Himalayan Plateau and over Leh. Easterly midlevel flow formed a rear-inflow jet of the type described by Smull and Houze (1987) to organize convection triggered earlier by daytime heating over the Tibetan Plateau into the westward propagating MCS (Rasmussen and Houze, 2012; Kumar et al. 2014). Kotal et al. (2014) have likened the Leh event to the Uttarakhand flood. However, we will demonstrate that these two events were very different with respect to the synoptic and mesoscale conditions leading to the considerable amounts of precipitation. This study will show specifically that the Uttarakhand flood case was characterized by a midlevel trough in the westerlies extending abnormally far south to the Himalayas, with its region of upward air motion located directly over Uttarakhand. As will be shown below, this trough merged with a monsoon low over central India to produce the Uttarakhand flood. In contrast, the Leh event was associated with strong easterly flow sandwiched between an anomalously strong midlevel ridge over the Tibetan plateau and a very strong monsoonal low over northern India. Not only were the synoptic-scale factors different in these cases, but also the precipitation was of a markedly different nature. Whereas the Leh event was the sudden and quick passage of an intense deep convective MCS, the Uttarakhand storm had a precipitation pattern controlled by synoptic-scale conditions associated with a baroclinic wave trough combining with a monsoon low. The precipitation was of a weaker, somewhat convective but more persistent nature.

Our paper was thus motivated in part by the need to correct a previously published mischaracterization of a meteorological event of great societal impact. We were not the first to note that another interpretation was needed. Unknown to us until the time of this writing, Ranalkar et al (2016) have also been re-analyzing the conditions associated with the Uttarakhand flood, and they have reached some conclusions about the synoptic-scale aspects of the storm that are generally consistent with those we present here. We encourage examination of their paper. However, we carry the analysis further by examining the dynamics of the storm in more detail, identifying separately the synoptic, mesoscale, convective, and land surface components of the

storm. In addition, we compare the Uttarakhand case to other recent major flood situations. Our results reinforce the position taken by Doswell et al. (1996) that local forecasting of flood situations is ideally based on identifying key meteorological and hydrologic "ingredients" and that a wide variety of synoptic and mesoscale situations can provide these ingredients.

#### 2. Data

### 2.1 Synoptic data

The National Center for Environmental Prediction/National Center for Atmospheric Research (NCEP/NCAR) reanalysis data was used on a 2.5° x 2.5° grid to investigate the meteorological and climatological conditions in the region of interest. ERA-Interim reanalysis data was used to investigate the structure of the dynamical tropopause for the event by plotting potential temperature on the 2 PVU surface, which is defined as the surface on which potential vorticity takes the value 2 PVU (1 PVU=10<sup>-6</sup> m<sup>2</sup> s<sup>-1</sup> K kg<sup>-1</sup>) in the Northern Hemisphere (Morgan and Nielsen-Gammon 1998). Specifically, these data are used to determine the large-scale synoptic features that define the environment in which the flood event occurred. Daily data were used to create mean composite and seasonal anomaly patterns from 13-18 June 2013 of geopotential height, winds, and precipitable water. In addition, quasigeostrophic Q-vectors (Hoskins et al. 1978; Hoskins and Pedder 1980; Durran and Snellman 1987; Sanders and Hoskins 1990), as well as O-vector divergence and convergence were calculated at 500 hPa using NCEP/NCAR reanalysis data for 17 June, the day the flooding occurred. Q-vectors are helpful in understanding the factors contributing to the vertical motion associated with the synoptic system that led to the flooding in Uttarakhand. As will be discussed below, the Qvectors help us to diagnostically separate synoptic factors from orographic, convective, and mesoscale factors at work in the Uttarakhand flooding event. We also have used NCAR/NCEP reanalysis in comparing with the Leh flood case in Section 7.

## 2.2 Satellite and radar data

The data used in this study are:

- Version 7 TRMM Precipitation Radar (PR) 2A25 data –Horizontal and vertical crosssections of the TRMM PR reflectivity data are used investigate the three-dimensional characteristics of the precipitating systems causing the floods.
- 3B42—TRMM-adjusted merged infrared precipitation estimates (three-hourly rainfall data; Huffman et al. 2007) were used to calculate accumulated rainfall over the Uttarakhand region. The use of the merged TRMM-adjusted dataset was necessary, because the TRMM satellite by itself has limited areal coverage of this region every day.
- Radar reflectivity data from the New Delhi Indira Gandhi International Airport is used to show the orographic effects of the Himalayas on the precipitation at the time of the flood event.
- Meteosat-7 infrared satellite imagery is used to examine the evolution of the clouds during the flood event and to provide context for the radar analysis.

## 3. Models used in the study

### 3.1 Mesoscale simulations

The Weather Research and Forecasting (WRF) Advanced Research WRF (ARW) model

version 3.5 (Skamarock et al. 2008) was used in two simulation frameworks to examine the (1) mesoscale and (2) synoptic perspectives of the Uttarakhand flood event. The WRF model is a compressible, non-hydrostatic, and three-dimensional mesoscale model. Both simulation sets were initialized with FNL NCEP data and were run for 48 h starting at 0000 UTC 16 through 0000 UTC 18 June 2013. The first simulation (1) was run with a triple-nested domain at 9, 3, and 1 km resolution (Figure 2a) and was used to investigate the mesoscale aspects of the flood event. The second simulation (2) was run with a double-nested domain at 81 and 27 km resolution (Figure 2b) and was used to produce the large-scale synoptic and Q-vector comparisons to reanalysis data. With both of these simulation sets, we are able to diagnose processes on scales ranging across synoptic, mesoscale, and convective scales. In addition, the Thompson et al. (2008) microphysics scheme was used for both sets of simulations because it has been shown to reproduce precipitating systems with both convective and stratiform precipitation in this part of the world and elsewhere (Kumar et al. 2014; Rasmussen and Houze 2016). Simulated radar reflectivity was estimated from the WRF model in simulation set (1) using the newly implemented Blahak (2007) methodology that uses direct microphysics assumptions and constants to calculate reflectivity. The specific physics options used in both simulation sets are summarized in Table 1.

## 3.2 Land Information System

Previous research on significant floods in this region has highlighted the role of soil moisture preconditioning and land surface interactions on these high-impact flood events (Kumar et al. 2014). To obtain soil moisture conditions for this study, we used the Land Information System (LIS), which is a land surface model developed at NASA Goddard. The LIS uses a data assimilation framework developed to produce optimal fields of land surface states and fluxes (Kumar et al. 2006; Peters-Lidard et al. 2007; Mohr et al. 2013). We ran the LIS offline at 3 km spatial resolution over the Uttarakhand region (same 3-km domain (d02) in simulation set (1) from Figure 2a) and used the Noah Land scheme (Ek et al. 2003) to reproduce soil moisture conditions in response to meteorological forcing fields obtained from the Global Data Assimilation System (GDAS). However, note that the LIS was not coupled to WRF in this analysis and was only run in the offline mode to investigate the long-term soil moisture characteristics in the Uttarakhand region. The LIS simulation was conducted from 1 January 2012 to 30 June 2013. This long offline simulation ensures that the land surface states simulated by the land surface model had adequate time to reach thermodynamic equilibrium with the forcing meteorology.

# 4. Characteristics of the clouds, precipitation, and soil moisture associated with the Uttarakhand flood

Before diagnosing the causes of the storms producing the Uttarakhand flood, we first summarize the nature of the clouds and precipitation that occurred during the days leading up to and during the event. Figure 3a shows that at 0000 UTC on 11 June 2013, a massive convective event produced a gigantic cold cloud shield over the Himalayas. This event contributed several hundred millimeters of rainfall to the region of Uttarakhand. The rain gauge network in the Himalayas is sparse; however, the rainfall leading to the Uttarakhand flood is shown by satellite remote sensing. Figure 4a, based on the TRMM 3B42 merged satellite product, shows the amount of precipitation that fell in the Uttarakhand region during 7-13 June, the period leading up to the flooding and landslides. Several hundred millimeters fell on the normally arid Himalayan slopes during that period. The convective storm shown in Figure 3a was the main

contributor to that rainfall.

The clouds and weather occurring during the four days immediately preceding and including the day of the flood (14-17 June) were very different than those of the earlier convective event shown in Figures 3a and 4a. Figure 3b exemplifies the cloud pattern during the flood period. An extensive cold cloud shield did not appear over Uttarakhand during the days of the flood, indicating that the precipitating clouds did not generally penetrate to high altitudes; i.e. the vertical motions were much less intense on the whole. Nevertheless, Figure 4b shows that during 14-17 June, the accumulation of precipitation was even greater than that associated with the prior convective event—over 300 mm fell throughout the entire state of Uttarakhand, with approximately 600-900 mm accumulations in the central part of the region. This massive amount of rainwater flowed down the already saturated mountainsides and was funneled into the intervening valleys to create the disastrous flooding and landslides.

The impact of the rainfall on the soil in the Uttarakhand region is indicated in Figure 5, which shows the rainfall rate and soil moisture time series obtained by averaging results from LIS (Section 3) for the four locations shown in Figure 1b for the period leading up to and including the time of the Uttarakhand flood. The soil moisture was very low in the first week of June, before multiple raining episodes. The LIS results indicate that the rainfall on 10 June (Figures 4a and 5b) caused the soil moisture over Uttarakhand to double suddenly (Figure 5a). After the first rain event a succession of spikes in soil moisture occurred in response to subsequent rainfall episodes, and the soil moisture remained high. This wetting of the soil by the convective storm would have made the mountainsides much more susceptible to runoff and landslides by the time of the Uttarakhand flood. After 15 June, the soil moisture was nearly saturated. It is therefore not surprising that the mountainsides around Uttarakhand became susceptible to the landslide and mudslide conditions that occurred in connection with the Uttarakhand flood episode.

## 5. Synoptic and mesoscale setting

To understand the atmospheric events that led to the storm that produced the extensive flooding in Uttarakhand, we first look at the large-scale flow pattern at 500 hPa over the European-Asian sector. On 10 June 2013, at about 50°N, three waves in the westerlies were located between western Europe and eastern Asia, and a strong ridge dominated over the Tibetan Plateau and the Hindu Kush mountains of Afghanistan (Figure 6a). The mid-tropospheric flow at Uttarakhand (gold star) at the time of the convective storm shown in Figure 3a was thus easterly, and no large-scale trough was affecting the region.

On 14 June 2013 (Figure 6b), a southwest-northeast oriented short-wave trough in the westerlies was "digging" southward to about 35°N between ~60 and 85°E and reached the northernmost tip of India, to the northwest of Uttarakhand. At the same time a closed cyclonic circulation was located along the eastern coast of India at about 20°N, 80°E. This low was of the type that frequently occurs over the Bay of Bengal during the monsoon and moves west to west-northwestward across the subcontinent (Shukla 1978).

On 17 June 2013, when the Uttarakhand floods were occurring, the trough in the westerlies extended still farther south, into India (Figure 6c), and the southwesterly flow ahead of the trough was located directly over Uttarakhand. In addition, the trough in the westerlies had merged with the monsoonal low to the south, so that the merged trough extended south to  $\sim 10^{\circ}$ N over the Arabian Sea. This merger of the eastward moving westerly trough and the lower latitude

westward moving low formed a hybrid storm, somewhat analogous to an extratropical transitioning tropical cyclone, with the additional effect of orographic lifting over the Himalayas. As we will see below, this combination of effects produced a kind of "perfect storm" directly over Uttarakhand. Ranalkar et al. (2016) also noted that the trough combined with the monsoonal low and that this combination was important for synoptic-scale moisture transport into the region of the flood.

We have seen that large precipitation amounts occurred during period of flooding (Figure 4b), but that the clouds (Figure 3b), were of a moderate nature, unlike those of the extreme convection seen on 10 June 2013 (Figure 3a). Figure 7 shows another view of the synoptic conditions on the highly convective day of 10 June 2013. The 700-hPa wind over Uttarakhand was from the northwest, and extremely dry air was being advected over the region from the highlands of the Hindu Kush mountains of Afghanistan and Pakistan. At 850 hPa, the wind was also from northwest, but it was advecting moist air from the Arabian Sea. This layering of the flow patterns is similar to typical situations leading to intense convection over northeastern India and Pakistan in which low-level moist air from the Arabian Sea is capped by subsiding midlevel air from the Afghan Plateau (Sawyer 1947; Houze et al. 2007; Romatschke et al. 2010). The intense convection along the Himalayan escarpment on 10 June 2013 is typical of that type of synoptic situation in which orographic lifting lifts the low-level moist air and releases the potential instability of the capping. However, these events were occurring a week before the Uttarakhand floods, and the synoptic situation changed radically in the coming days.

Figure 8 is in the same format as Figure 7, and comparison of these two figures shows the stark difference in the synoptic environment on the day of the flood compared to that of the convective event in the previous week. Figure 8a shows that the 700 hPa wind at Uttarakhand was perpendicular to the Himalayan escarpment and advecting highly anomalously moist air into the region from the Arabian Sea. The 850 hPa wind (Figure 8b) was also southerly and perpendicular to the Himalayas and was advecting moisture into the region from the Arabian Sea. The southerly direction of the wind at both 850 and 700 hPa was consistent with Uttarakhand lying just to the east of the 500 hPa trough line seen in Figure 6c.

The midlatitude influence of the flow over Uttarakhand on 17 June 2013 is further shown by Figure 9, which contains a sequence of ERA-interim 2 PVU (tropopause) plots of potential temperature ( $\theta$ ) for 13, 15, and 17 June (Figures 9a-c). Tropopause potential temperature maps indicate the variation in the height of the tropopause in potential vorticity coordinates. The low tropopause potential temperature shown in blue colors progressively extends southward in a westward moving and amplifying trough. The packing of contours at the border of the blue shading indicates the westerly jet location. The jet remained north of Uttarakhand although the merger with the monsoonal low (Figure 6) extended the trough and subsequent southwesterly flow into the Uttarakhand region considerably farther south.

The trough is clearly evident in the 500 hPa mean heights for 17 June 2013 (Figure 10). Also shown are contours of the forcing term in the quasi-geostrophic Omega equation,  $-2\nabla \cdot \mathbf{Q}$ , where  $\mathbf{Q}$  is the quasi-geostrophic Q-vector. Red contours in Figure 10 indicate regions of positive forcing due to Q-vector convergence. They show that on this day Q-vector convergence was contributing to upward motion east of the trough line as it was moving over the Uttarakhand flood area. According to quasi-geostrophic reasoning (Holton and Hakim 2013), the areas of converging (diverging) Q-vectors indicate rising (subsiding) motion due to synoptic-scale forcing. The blue contours indicate areas of large-scale Q-vector divergence west of the trough

line.

At these latitudes, quasi-geostrophic balance may not be exact but authors such as Sanders (1984) and Shaevitz et al. (2016) have provided evidence that quasi-geostrophic balance at least partially applies in this region. The Q-vector divergence/convergence pattern in Figure 10 indicates that the trough in the westerlies combined with the monsoonal low to the south was producing a degree of synoptic scale upward forcing directly over Uttarakhand during the time period of the flood. Figure 11 shows that the lower-resolution WRF simulation (d01; Figure 2b) also captured the Q-vector convergence and vertical motion over the flood zone at 0600 UTC 17 June 2013. The red and blue shading in Figure 11 shows the upward and downward motion, respectively, computed by inverting the Q-vector convergence, without orographic or boundary layer forcing (RIP program; http://www2.mmm.ucar.edu/wrf/users/docs/ripug.htm). This model result together with the NCEP reanalysis data indicate that upward air motion associated with the synoptic-scale pressure pattern was optimally positioned over Uttarakhand at the time of the storm that produced the flooding. Thus, synoptic-scale lifting was a contributor to the storm producing the flood and explains the long, roughly 3-day duration of the storm as the trough slowly passed over the region on 15-18 June.

## 6. Vertical motion and thermodynamics on the day of the flood

Figure 12 is a plot of the 1-km resolution WRF (d03; Figure 2a) model vertical velocities at 500 and 700 hPa, where red shading denotes rising motion and the black vectors are horizontal winds at 0600 UTC on 17 June. Notable at both 500 and 700 hPa is the line of intermittent updraft motion aligned with the approaching baroclinic trough seen in Figures 10 and 11. The wind vectors in Figure 12b show the lower-level cyclonic circulation associated with the trough behind the line of upward motion. In association with the low, the model simulations captured the northward turning of the winds into the Himalayas, which is consistent with the baroclinic wave trough being in the region. Also notable in the 500 hPa vertical velocities is that as the system reaches the Himalayas, the warm, moist air that was being advected from the Arabian Sea was orographically lifted over a much broader region when it reached the steep Himalayan terrain. This broader region of uplift was likely key to the massive condensation and accumulation of precipitation in the flood region. Because this flow pattern was associated with the synoptic situation this orographic component of lifting was persistent over a 2-3 day period. Persistence of lifting is a factor that has been identified as a key ingredient in other notable floods around the world (see Section 7).

An important question is, how stable was the air as it rose over the Himalayas? Operational soundings are not available for the region directly upstream of the mountains in the area of interest to this study. However, we have obtained an indication of the stability from soundings reconstructed from the WRF output. Figure 13 shows model soundings at points A and B located upstream of the terrain in Figure 12. At point A, farther upstream, the temperature buoyancy of an undiluted parcel was ~5°C through most of the troposphere (Figure 13a). That thermal profile was consistent with the line of intermittent cellular vertical motion upstream of the mountain range. The northern point B is in the lower foothills, and the sounding in Figure 13b was closer to moist adiabatic. The air was probably more thoroughly mixed by prior convection. Farther north in the broader area of lifting over the windward slope (Figure 12), the soundings were saturated and moist neutral (not shown). Ranalkar et al. (2016) used satellite products to show that lightning existed in the region. It is well known that lightning can occur in stable as well as unstable lifting as long as graupel is present. Thus, the presence of lightning in

the satellite data case does not establish that the precipitation was entirely convective in nature. Importantly, these soundings from the cloud-resolving model simulation indicate that by the time the air was rising over the terrain, the thermodynamic profile was neutral, implying the embedded moderate convection was mostly upstream of the area of flooding. The lifting over the flooded areas was mostly of a stable nature.

### 7. Radar echoes and vertical structure

An analysis of the three-dimensional structure and dynamics of the precipitating systems that produced the Uttarakhand flood is helpful for understanding the nature of this high-impact event. Precipitation radar data from the TRMM PR have been especially useful for characterizing convective and stratiform precipitation in terms of the vertical and horizontal structures of radar echoes over low latitudes (Houze et al. 2007; Romatschke et al. 2010; Romatschke and Houze 2010; Rasmussen and Houze 2011; Houze et al. 2015). These prior papers have identified three radar echo categories as defining the most extreme forms of convection over land; these categories are deep convective cores (DCCs; 40 dBZ echoes reaching > 10 km height), wide convective cores (WCCs; 40 dBZ echoes exceeding 1000 km² in contiguous horizontal extent), and broad stratiform regions (BSRs; stratiform echoes extending contiguously >50,000 km²). An objective search of TRMM radar echoes for the time period and region of the Uttarakhand flood showed no TRMM radar echoes that could be classified as DCC, WCC, or BSR, whereas previous India/Pakistan floods that we have studied were all associated with these extreme forms of echo. Thus, we conclude that the convection in the case of the Uttarakhand flood was not extreme by these previously used standards.

The precipitation radar on the TRMM satellite shows only occasional snapshots of the three-dimensional radar reflectivity. Figure 14 shows the display of radar reflectivity as detected by the ground-based operational radar at the New Delhi Indira Gandhi International Airport at 0742 UTC 17 June 2013, on the day of the Uttarakhand flood. This radar image is typical of the echo pattern during the period of the flood; a line of precipitation was paralleling the leading edge of the wave trough, in the zone of upward motion associated with the wave. This pattern suggests that wave trough dynamics were organizing the precipitating clouds in a quasi-linear fashion, consistent with Figure 12. Near the foothills, the precipitation area widened. The widening could have been partially due to the increasing height of the radar beam with increasing range from the radar. However, the widening also corresponds well to the area where the lifting ahead of the wave trough was being enhanced in a broad region by flow over the Himalayan terrain (Figure 12).

The TRMM PR captured the vertical structure of the precipitating system over Uttarakhand during the day of the flood. Figure 15 shows Meteosat-7 infrared imagery and TRMM PR data over Uttarakhand during a TRMM overpass at 0715 UTC on 17 June. Figure 15b shows the TRMM PR echo in a cross section along the white line in Figure 15a. The highly convective India and Pakistan flood events of 2010-2012 described by Rasmussen et al. (2015, see their Figure 8) had cloud-top temperatures mostly ~20 K colder than those associated with the Uttarakhand flood precipitating system (Figure 15a). The vertical cross-section obtained from a TRMM PR overpass in Figure 15b shows that the structure of the system over Uttarakhand was generally stratiform in nature with embedded convection along the mountainous foothills, where instability was still being released in the air moving over the terrain. The embedded convection was not penetrating to great heights, which explains the general lack of very high cloud tops in Figure 15a. In the highly convective cases described by Rasmussen et al. (2015), regions of deep

convection with reflectivity values > 35 dBZ reached at least 10 km, whereas in the Uttarakhand storm, the same reflectivities only reached ~7 km in height.

The reflectivity cross-section computed from the 1-km resolution WRF simulation (Figure 15c) was consistent with the TRMM PR cross section in Figure 15b. The TRMM cross section was truncated before it intersected the mountains because of problems with the radar data near the terrain. However, the cross section of model output shows the bright band sloping downward into the mountainside terrain (Figure 15b). Such a downward sloping brightband is often seen in radar data in stratiform regions over mountains (e.g. in OLYMPEX, http://olympex.atmos.washington.edu/) and is probably due at least in part to cooling by the lifting over the terrain. A feature notable in the Uttarakhand storm was the presence of widespread snowfall at higher altitudes in the Himalayas. Members of the Kailash pilgrimage in the higher terrain were blinded by continuous driving snow on 17 June 2013 (reported photographically to the authors by Professor David Battisti, who was on the pilgrimage; personal communication). The intersection of the bright band with the mountains indicates that the higher terrain was receiving snowfall consistent with the observations of the pilgrims.

## 8. Comparison with other recent flood events

The Uttarakhand flood is distinctly unlike other recent notorious floods in the Himalayan region in recent years. Rasmussen et al. (2015) described the large-scale conditions and mesoscale characteristics of the storms producing several of the major floods of 2010-2012. These storms were associated with a strong flow concentrated between abnormally high pressure over the Tibetan Plateau and a monsoon low extending anomalously far westward over northern India. That synoptic pattern contrasts sharply with the westerly trough dominating the Uttarakhand flood case.

In the 2010-2012 cases examined by Rasmussen et al. (2015), strong flow between the high over Tibet and the low over India advected large amounts of moisture into the region just south of and over the Himalayas. This moist flow facilitated deep convective MCSs with trailing stratiform precipitation of the type described by Houze (2004). The floods in the 2010-2012 cases were produced by these deep convective MCSs, in contrast to the more moderate clouds and precipitation of the Uttarakhand flood.

The Pakistan/India floods described in the Rasmussen et al. (2015) paper were all of the slow-rising type. Another type of flood occurred over Leh, India, in 2010. It was a flash flood that occurred suddenly in the high-altitude terrain of the Indus River valley at the city of Leh in India (Rasmussen and Houze 2012). This flash flood was due to the passage of a deep convective MCS that formed over the Tibetan Plateau and moved rapidly westward over Leh. Figure 16a is an infrared satellite image showing the storm that produced the Leh Flood. It had an extremely cold cloud top, similar to that on the 10 June 2013 Uttarakhand storm (Figure 3a) and utterly unlike the clouds of the 17 June Uttarakhand flood case (Figure 3b). Figure 16b shows the 500-hPa winds, which illustrate how this case was associated with anomalously strong ridge over the Tibetan Plateau, with easterly flow directed toward and over Leh. Figure 16b also includes contours of the deviation of the 500-hPa height from its seasonal value, illustrating that the flow pattern in the Leh case was highly anomalous for the season. The Uttarakhand case was also unusual; however, its abnormality was in the form of the excursion of a synoptic-scale westerly trough into India, while the Leh case was abnormal for its ridging and easterly flow. The 500-hPa easterlies in the Leh case were directed into the trailing stratiform region of the MCS that

caused the flooding in Leh. It formed a rear inflow jet of the type associated with rapidly propagating leading-line/trailing stratiform squall lines (Smull and Houze 1987). This synoptic situation could hardly be more different than that of the westerly trough associated with the Uttarakhand flood. Characterizing these two flood situations as similar (e.g. Kotal et al. 2014) is

clearly incorrect. The only characteristic that we have found that these two flood cases had in common is the pre-moistening of the soil (described in Section 6 above) by rain occurring in several days immediately preceding the flood. Yet it is important to note that both flow situations were highly anomalous for the season in which they occurred.

Two flood situations that have more in common with the Uttarakhand flood are the Colorado and Alberta floods of 2013, which have been investigated by Gochis et al. (2015), Milrad et al. (2015), and Friedrich et al. (2016). These authors point out that these floods were associated with low-level synoptic and mesoscale flow on the north sides of cyclonic circulations and that such circulation patterns are highly anomalous for the season in which they occurred. Further illustrating the anomalous character of the synoptic situation in the Colorado case, Gochis et al. (2015) found that the operational radar reflectivity to rain rate (Z-R) relationship routinely used for this midlatitude location underestimated the rainfall by a factor of two, but when the formula was changed to a tropical Z-R relationship, the radar-based rain estimates were much closer to the observed precipitation amounts. The North American cases, however, did not resemble the Uttarakhand case in all respects; Gochis et al. (2015) noted that the low-level cyclonic circulation in the Colorado case was associated with a cutoff low at midlevels, not an upper-level open-wave trough like that which propagated into and through the Uttarakhand region. Moisture, however, was concentrated at low levels, and the persistent easterly flow patterns in the Colorado and Alberta flood cases advected moist air toward the Rocky Mountains for a sustained period of time as was the case in Uttarakhand. Rain rates were not notably large in either the Uttarakhand or Rocky Mountain events, nor were the airflows especially unstable. Milrad et al. (2015) found that the "quasi-geostrophic and orographic ascent in Alberta acted to release conditional instability in a moderate CAPE environment during the first part of the event (0000–0600 UTC 20 June), before a transition to moist-neutral ...". This behavior of the lowlevel moist flow field is very similar to that which we have described for the Uttarakhand flood. In addition, the nature of the precipitation was similar. Friedrich et al. (2016) found moderate convective cells on the lower slopes of the Rockies, with warm coalescence processes dominating precipitation processes at lower levels and ice processes contributing above the melting level when the instability was moderate. These radar echo characteristics resemble those seen in the Uttarakhand case

### 9. Conclusions

From 13-17 June 2013, a trough in the westerlies extended southward into northern India. Such southward intrusion of a westerly trough is unusual in this region and season. The eastward moving trough in the westerlies merged with a monsoonal low moving westward across India, producing a "perfect storm" in which a low-level warm moist jet was advecting abnormally moist warm air directly toward the Himalayan escarpment from the Arabian Sea into Uttarakhand. These synoptic facts were noted by Ranalkar et al. (2016). Orographic forcing combined with upward motion associated with the wave in the westerlies converted the moisture flux to heavy, continuous precipitation over the region. The LIS showed that the mountainsides had been pre-moistened by prior storms in the immediately preceding week, and the heavy rainfall running down the valleys of Uttarakhand led to flooding and landslides. Being associated

with a trough in the westerlies sharply distinguished this flood from the Leh flood of 2010. Previous studies asserting that the Leh and Uttarakhand floods were similar weather situations are incorrect.

Infrared satellite imagery showed the Uttarakhand floods were caused by a cloud system with relatively warm cloud tops, unlike storms in more convective flood cases. TRMM PR observations on the day of the flood showed no extreme forms of convective echo of the types identified in other flood cases in India/Pakistan, and indicated rather that the precipitation was broadly stratiform, with snow at high elevations, but the storm nonetheless had embedded, though not especially deep, convection along the lower slopes of the Himalayas. The fact that this case was not dominated by deep convection distinguished it not only from the Leh flood case but also from other recent major floods in Pakistan and Northwest India, which have been caused by highly convective storm systems with very deep and intense convective elements.

From these results and those of previous studies, it is clear that very different types of storms can produce flooding in northern India and Pakistan and other mountainous regions. Most of the recent floods in India and Pakistan have been of an intense convective nature, with mesoscale convective systems playing the dominant role. In this case, it was a trough in the westerlies combined with a monsoonal low that did not trigger a lot of deep or otherwise extreme convection, but rather induced a persistent and narrowly concentrated zone of low-level moist flow impinging directly on the Himalayas in the region of Uttarakhand. Because of the long timescale of the synoptic-scale baroclinic system and the forcing of its low-level jet over the terrain for many hours, a great amount of moisture could be converted to precipitation in this manner over the ridges and valleys of the Himalayan escarpment. Precipitation during the week preceding the storm over Uttarakhand state had greatly moistened the soil in the region, and one of the most devastating floods in India's history occurred.

Recent major floods in Colorado and Alberta in 2013 had some features in common with the Uttarakhand flood. They both had low-pressure systems that directed low-level moist flows into the Rocky Mountains for many hours, similar to the persistent low-level flow advecting moist air into the Himalayas in the event of the Uttarakhand flood. The low-level flow in the case of the Uttarakhand flood was occurring in connection with the passage of a trough in the westerlies that extended unusually far southward and joined with a monsoonal low. The Colorado and Alberta cases also occurred under highly abnormal flow conditions for the season, albeit in the Colorado case the upper-level flow was a cutoff low rather than a transitory trough. Other major floods in India/Pakistan have included both flash floods and slow-rise floods due to the occurrence of intense mesoscale convective systems, often with a ridge over the Tibetan Plateau and a pronounced monsoon low extending across north India. These floods were associated with extreme forms of convection marked by radar echoes identified in TRMM radar data; such extreme echo forms were absent in the region and time period of the Uttarakhand flood. These various synoptic situations and different forms of convection implicated in major floods in different mountainous regions of the world caution strongly against analog forecasting and point to the essential approach for forecasters that was laid out by Doswell et al. (1996), namely, that one should focus on the meteorological "ingredients" of a flood situation. More specifically, forecasters should look for those synoptic and mesoscale situations where ascent of air and high moisture content combine with the speed of storm movement and duration to maximize the output of rain on a given watershed. As pointed out by Doswell et al. (1996), such ingredients can occur in diverse synoptic and mesoscale situations. We would suggest based on

our LIS calculations that soil moisture preconditioning by prior storms in the area in a vulnerable watershed is a hydrologic ingredient that should be taken into account along with the meteorological ingredients.

In addition, we suggest that the vigilance for ingredients on a day-to-day basis could be aided by continual monitoring for anomalous flow patterns. The India/Pakistan floods of 2010-2012 (Rasmussen et al. 2015), the Leh flood (Rasmussen and Houze 2012), and the Colorado and Alberta Floods (Gochis et al. 2015; Milrad et al. 2015; Friedrich et al. 2016) all occurred in highly abnormal circulation patterns for their respective regions and seasons. The combination of abnormality of flow, meteorological ingredients, and pre-moistening of ordinarily dry soil in mountainous environments might be the best set of factors to consider when identifying a potentially damaging and dangerous flood situation.

## Acknowledgements

This research was sponsored by National Science Foundation grant AGS-1503155, National Aeronautics and Space Administration grant NNX16AD75G, and a National Center for Atmospheric Research Advanced Study Program (ASP) postdoctoral fellowship. Beth Tully coordinated artwork and graphics and edited the text. Professor Steven Cavallo provided the tropopause potential temperature maps.

### **REFERENCES**

- Blahak U. 2007. RADAR\_MIE\_LM and RADAR\_MIELIEB Calculation of radar reflectivity from model output. Tech. Rep., Instit. For Meteor. and Climate research, Univ./Research Center Karlsruhe, 150pp
- Chen F, Dudhia J. 2001. Coupling an advanced land-surface/hydrology model with the Penn State/NCAR MM5 modeling system. Part 1: Model implementation and sensitivity. *Mon. Wea. Rev.*, **129**, 569-585.
- Doswell CE III, Brooks HE, Maddox RA. 1996. Flash flood forecasting: An ingredients-based methodology. *Weather and Forecasting*, **11**: 560–581.
- Dudhia J. 1989. Numerical study of convection observed during the Winter Monsoon Experiment using a mesoscale two-dimensional model. *J. Atmos. Sci.*, **46**, 3077-3107.
- Durran DR, Snellman LW. 1987. On the diagnosis of synoptic-scale vertical motion in an operational environment. *Wea. and Forecasting* **2**: 17–31.
- Ek MB, Mitchell KE, Lin Y, Rogers E, Grunmann P, Koren V, Gayno G, Tarpley JD. 2003. Implementation of Noah land surface model advances in the National Centers for Environmental Prediction operational mesoscale Eta model. *J. Geophys. Res.* **108**: 8851. doi:10.1029/2002JD003296.
- Friedrich K, Kalina EA, Aikins J, Gochis D, Rasmussen R. 2016. Precipitation and cloud structures of intense rain during the 2013 Great Colorado Flood. *J. Hydrometeorol.* 17: 27–52.
- Gochis D, Schumacher R, Friedrich K, Doesken N, Kelsch M, Juanzhen Sun J, Kyoko Ikeda K, Lindsey D, Wood A, Dolan B, Matrosov S, Newman A, Mahoney K, Rutledge S, Johnson R, Paul Kucera P, Kennedy P, Sempere-Torres D, Steiner M, Roberts R, Wilson J, Yu W. Chandrasekar V, Rasmussen R, Anderson A, Brown B. 2015. The Great Colorado Flood of September 2013. *Bull. Amer. Meteor. Soc.* **96:** 1461–1487.
- Holton JR, Hakim GJ. 2013. An Introduction to Dynamic Meteorology. Academic Press (or would it be Elsevier?) 5<sup>th</sup> Ed., New York (or should it be London or Amsterdam?), 532pp.
- Hong S-Y, Noh Y, Dudhia J, 2006. A New vertical diffusion package with an explicit treatment of entrainment processes. *Mon. Wea. Rev.*, **132**, 2318-2331.
- Hoskins BJ, Pedder MA. 1980. The diagnosis of middle latitude synoptic development. *Q. J. R. Meteorol. Soc.* **106**: 707–719.
- Hoskins BJ, Draghici I, Davies HC. 1978. A new look at the omega-equation. *Quart. J. Roy. Met. Soc.* **104**: 31–38.
- Houze RA Jr, 2004. Mesoscale convective systems. *Rev. Geophys.* **42**: 10.1029/2004RG000150, 43 pp.
- Houze RA Jr, Wilton DC, Smull BF. 2007. Monsoon convection in the Himalayan region as seen by the TRMM Precipitation Radar. *Quart. J. Roy. Meteor. Soc.* **133**: 1389–1411.
- Houze RA Jr, Rasmussen KL, Zuluaga MD, Brodzik SR. 2015. The variable nature of

- convection in the tropics and subtropics: A legacy of 16 years of the Tropical Rainfall Measuring Mission (TRMM) satellite. *Rev. Geophys.* **53**: doi:10.1002/2015RG000488.
- Houze RA Jr, Rasmussen KL, Medina S, Brodzik SR, Romatschke U. 2011. Anomalous atmospheric events leading to the Summer 2010 floods in Pakistan. *Bull. Amer. Meteor. Soc.* **92**: 291–298.
- Huffman GJ, Adler RF, Bolvin DT, Gu G, Nelkin EJ, Bowman KP, HongY, Stocker EF, Wolff DB. 2007. The TRMM multi-satellite precipitation analysis: Quasi-global, multi-year, combined-sensor precipitation estimates at fine scale. *J. Hydrometeorol.* **8**: 38–55.
- Kain JS, Fritsch JM. 1993. Convective parameterization for mesoscale models: The Kain-Fritsch Scheme. In *The Representation of Cumulus Convection in Numerical Models*, *Meteor. Monogr.*, **46**, Amer. Meteor. Soc., 165-170. DOI: 10.1007/978-1-935704-13-3 16.
- Kotal SD, Roy SS, Bhowmik RSK. 2014. Catastrophic heavy rainfall episode over Uttarakhand during 16–18 June 2013—observational aspects. Curr Sci 107:234–245.
- Kumar ARA, Houze RA Jr, Rasmussen KL, Peters-Lidard C. 2014. Simulation of a flash flooding storm at the steep edge of the Himalayas. *J. Hydrometeorol.* **15**: 212–228.
- Kumar SV, Peters-Lidard CD, Tian Y, Houser PR, Geiger J, Olden S, Lighty L, Eastman JL, Doty B, Dirmeyer P, Adams J, Mitchell K, Wood EF, Sheffield J. 2006. Land Information System: An interoperable framework for high resolution land surface modeling. *Environmental Modelling & Software*, **21**, 1402–1415.
- Milrad SM, Gyakum JR, Atallah EH. A meteorological analysis of the 2013 Alberta flood: Antecedent large-scale flow pattern and synoptic–dynamic characteristics. 2015. *Mon. Wea. Rev.* **143**, 2817–2841.
- Mlawer EJ, Taubman SJ, Brown PD, Iacono MJ, Clough SA. 1997. Radiative transfer for inhomogeneous atmospheres: RRTM, a validated correlated-k model for the longwave. J. of Geophys. Res., **102**, 16663-16682.
- Mohr KI, Tao W-K, Chern J-D, Kumar SV, Peters-Lidard CD. 2013. The NASA-Goddard Multi-scale Modeling Framework—Land Information System: Global land/atmosphere interaction with resolved convection. *Environmental Modelling & Software* **39**: 103–115.
- Morgan, MC, Nielsen-Gammon JW. 1998. Using tropopause maps to diagnose midlatitude weather systems. *Mon. Wea. Rev.* **126**: 2555–2579.
- Peters-Lidard CD, Houser PR, Tian Y, Kumar SV, Geiger J, Olden S, Lighty L, Doty B, Dirmeyer P, Adams J, Mitchell K, Wood EF, Sheffield J. 2007. High-performance Earth system modeling with NASA/GSFC's Land Information System. *Innovations Syst. Softw. Eng.*, **3**, 157-165. DOI 10.1007/s11334-007-0028-x.
- Ranalkar MR, Chaudlhari HS, Hazra A, Sawaisarje GK, Pokhrel S. 2016. Dynamical features of incessant heavy rainfall event of June 2013 over Uttarakhand, India. Nat. Hazards, 80, 1579-1601. DOI 10.1007/s11069-015-2040-z
- Rasmussen KL, Houze RA Jr. 2011. Orogenic convection in South America as seen by the TRMM satellite. *Mon. Wea. Rev.*, **139**, 2399-2420.
- Rasmussen KL, Houze RA Jr. 2012. A flash flooding storm at the steep edge of high terrain:

- Disaster in the Himalayas. Bull. Amer. Meteor. Soc. 93: 1713–1724.
- Rasmussen KL, Houze RA Jr. 2016: Convective initiation near the Andes in subtropical South America. *Mon. Wea. Rev.* In press.
- Rasmussen KL, Hill AJ, Toma VE, Zuluaga MD, Webster PJ, Houze RA Jr. 2015. Multiscale analysis of three consecutive years of anomalous flooding in Pakistan. *Quart. J. Roy. Meteor. Soc.* **141**: 1259–1276, doi:10.1002/qj.2433.
- Romatschke U, Houze RA Jr. 2010. Extreme summer convection in South America. *J. Climate* **23**, 3761–3791.
- Romatschke U, Medina S, Houze RA Jr. 2010. Regional, seasonal, and diurnal variations of extreme convection in the South Asian region. *J. Climate* **23**: 419–439.
- Sanders F. 1984. Quasi-geostrophic diagnosis of the monsoon depression of 5-8 July 1979. *J. Atmos. Sci.* 41: 538–552.
- Sanders F, Hoskins BJ. 1990. An easy method for estimation of Q-vectors from weather maps. *Weather and Forecasting* **41**: 538–552.
- Sawyer JS. 1947. The structure of the intertropical front over NW India during the SW monsoon. *Quart. J. Roy. Meteorol. Soc.*, **73**: 346–369.
- Shaevitz DA, Nie J, Sobel AH. 2016. The 2010 and 2014 floods in India and Pakistan: dynamical influences on the vertical motion and precipitation. Submitted to *J. Geophys. Res. Atmos.* [Available online at http://arxiv.org/abs/1603.01317]
- Shukla J. 1978. CISK-barotropic-baroclinic instability and the growth of monsoon depressions. *J. Atmos. Sci.* **35**: 495–508.
- Skamarock WC, Klemp JB, Dudhia J, Gill DO, Barker DM, Duda MG, Huang X-Y, Wang W, Powers JG. 2008. A description of the Advanced Research WRF version 3. NCAR Tech. Note NCAR/TN- 4751STR, 125 pp. [Available online at http://www.mmm.ucar.edu/wrf/users/docs/arw v3.pdf.]
- Smull BF, Houze RA Jr, 1987. Rear inflow in squall lines with trailing stratiform precipitation. *Mon. Wea. Rev.* **115**: 2869–2889.
- Thompson G, Field PR, Rasmussen RM Hall WD. 2008 Explicit Forecasts of Winter Precipitation using an improved bulk microphysics scheme. Part II: Implementation of a new snow parameterization. *Mon. Wea. Rev.*, **136**, 5096-5115.

## **Tables**

**Table 1.** WRF model setup for both simulation sets described in section 3.1.

Physical Process	Scheme	Reference
Microphysics	Thompson scheme; 6-class scheme with graupel, double moment for cloud ice	Thompson et al. (2008)
Longwave radiation	Rapid Radiative Transfer Model	Mlawer et al. (1997)
Shortwave radiation	Dudhia	Dudhia (1989)
Surface layer	Monin-Obukhov	
Land surface	Noah Land Surface Model	Chen and Dudhia (2001)
Planetary boundary layer	Yonsei University (YSU) PBL	Hong et al. (2006)
Cumulus convection	Kain-Fritsch, none in d03 in Figure 2a	Kain and Fritsch (1993)

## **FIGURE CAPTIONS**

- **Figure 1.** (a) Geography of the region of study. Uttarakhand state is colored red. (b) Uttarakhand state with locations of stations used to create Figure 5.
- **Figure 2.** WRF model nested domains at (a) 9-, 3-, and 1-km grid spacing, and (b) 81-, and 27-km grid spacing. The domain names, d01, d02, and d03 are also indicated on the figure. The white circle is centered in Uttarakhand.
- **Figure 3.** Meteosat-7 infrared satellite imagery for (a) 0000 UTC 11 June and (b) 0700 17 June 2013.
- **Figure 4.** Accumulated rainfall over Uttarakhand from TRMM 3B42 for the periods (a) 7-13 June 2013 and (b) 14-17 June 2013.
- **Figure 5.** NASA Goddard Land Information System (LIS) output with 3 km spatial resolution over the Uttarakhand region for month of June 2013. (a) Average rainfall rate in mm h<sup>-1</sup> (b) Average soil moisture (m³ of water per m³ of soil). Stations in the average are: Joshimath (30.56N, 79.57E), Uttarkashi (30.72N, 78.43E), Kedarnath (30.73N, 79.06E), and Almora (29.81N, 79.29E). See Figure 1b for locations.
- **Figure 6.** 500 hPa geopotential height (m) for (a) 10 June 2013, (b) 14 June 2013 and (c) 17 June 2013.
- **Figure 7.** 10 June 2013 (a) mean precipitable water anomaly (mm) and 700 hPa wind, and (b) mean specific humidity anomaly (kg kg<sup>-1</sup>) and 850 hPa wind. Anomalies are departures from the monsoon seasonal mean (June-September).
- **Figure 8.** As in Figure 7 but for 17 June 2013.
- **Figure 9.** (a)-(c) Sequence of ERA-interim 2 PVU (tropopause) plots of potential temperature (θ). Landmasses are outlined with heavy black borders. The dark line separating blue and orange shades occurs where the potential temperature lines are tightly packed and as such indicate the jet stream. The star shows the approximate location of the Uttarakhand flood.
- **Figure 10.** 500 hPa heights in meters (black contours) for 17 June 2013 from NCEP/NCAR reanalysis. Calculated Q-Vectors are shown in black vectors. Regions of Q-Vector convergence (red contours), and Q-Vector divergence (blue contours) indicate synoptic-scale areas of rising (sinking) motion. The red and blue contours have units of 10<sup>17</sup> m kg<sup>-1</sup> s<sup>-1</sup>. The star shows the location of the Uttarakhand flood.
- **Figure 11.** WRF model 500 hPa Q-vectors (black vectors). Upward motion (dPa s<sup>-1</sup>) implied by Q-vector convergence is in red shading. Downward motion implied by Q-vector divergence is in blue shading. The fields shown are for 0600 UTC 17 June 2013. The location of the Uttarakhand flood is denoted by the star.
- **Figure 12.** WRF simulation of vertical velocities (cm s<sup>-1</sup>) and horizontal winds (black vectors) for 0600 UTC 17 June 2013 for (a) 500 hPa, (b) 700 hPa. Red (blue) shading denotes upward (downward) vertical velocities. The points A and B indicate the locations of soundings shown in Figure 13.

- **Figure 13.** Soundings derived from WRF output for 0600 UTC 17 June 2013 for (a) point A and (b) point B in Figure MODELW. Temperature and dew point are displayed in Skew-T/Log-p format. The dashed red curves show the temperature of an undiluted parcel lifted from the surface.
- **Figure 14.** Low-level radar reflectivity (dBz) display from the operational radar at New Delhi Indira Gandhi International Airport (denoted by the airplane icon) at 0743 UTC 17 June 2013, during the Uttarakhand flood event. The color bar and image were available on the Indian Meteorological Department website. The star denotes the location of the Uttarakhand flood.
- **Figure 15.** (a) *Meteosat-7* satellite infrared brightness temperatures (K). Star denotes location of flooding. (b) Vertical cross-section of TRMM PR data in dBZ taken left to right along the white line in (a). (c) WRF Radar reflectivity (d03) computed along a similar cross section to Figure 15b (Figure 2a) at 0700 UTC 17 June 2013.
- **Figure 16.** (a) *Meteosat-7* satellite infrared image (K) for 2000 UTC 5 August 2010 from *Meteosat-7* showing the MCS that resulted in the Leh flood. The location of Leh is indicated by a circled cross. (b) 500 hPa winds at 1200 UTC 5 August 2010. Contours show the 500 hPa height deviation from the seasonal average. Adapted from Rasmussen and Houze (2012).

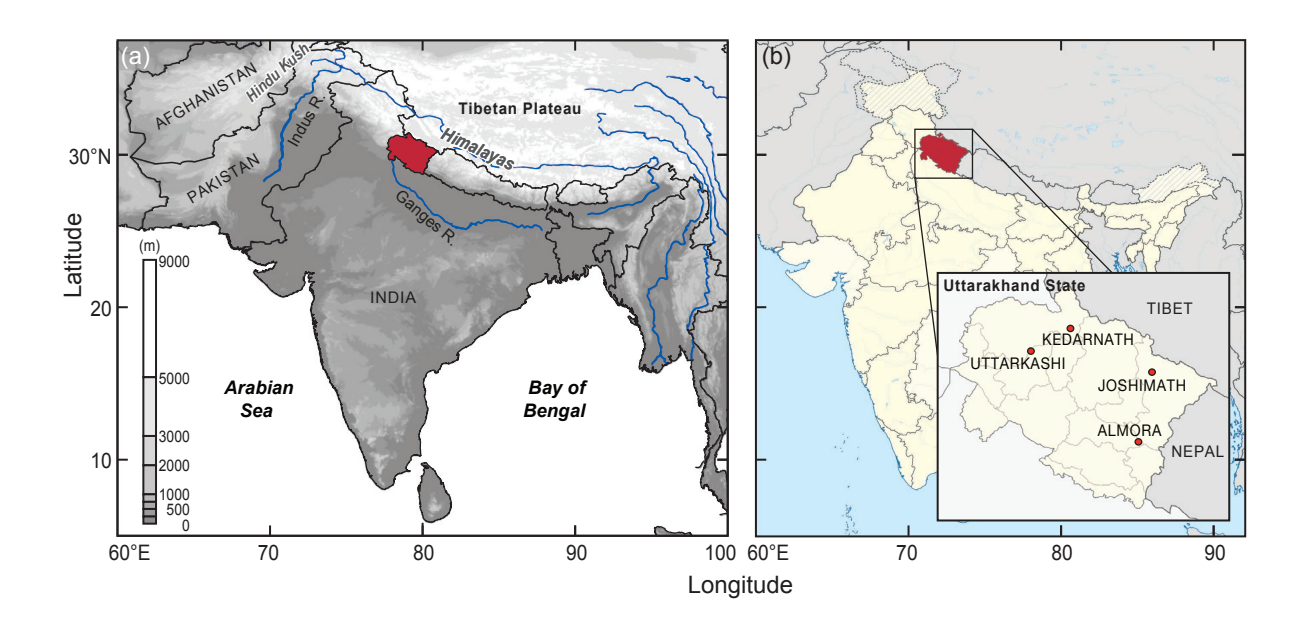


**Figure 1.** (a) Geography of the region of study. Uttarakhand state is colored red. (b) Uttarakhand state with locations of stations used to create Figure 5.

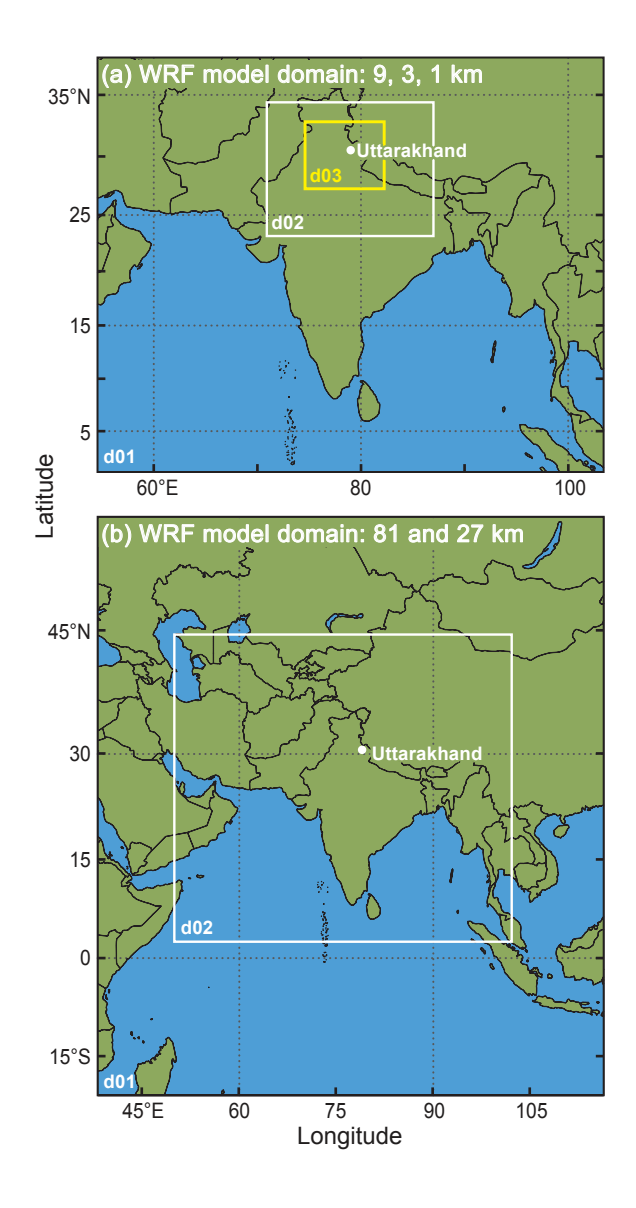


**Figure 2.** WRF model nested domains at (a) 9-, 3-, and 1-km grid spacing, and (b) 81-, and 27-km grid spacing. The domain, d01, d02, and d03 are also indicated on the figure. The white circle is centered in Uttarakhand.

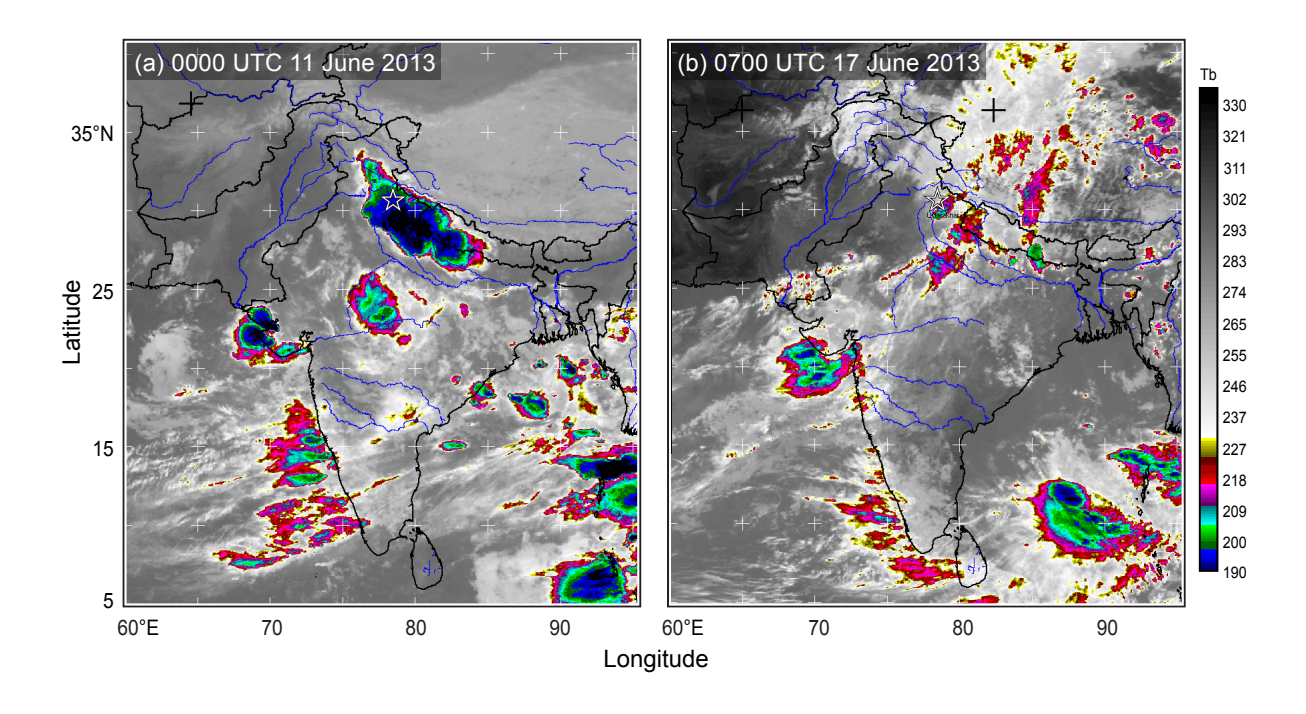
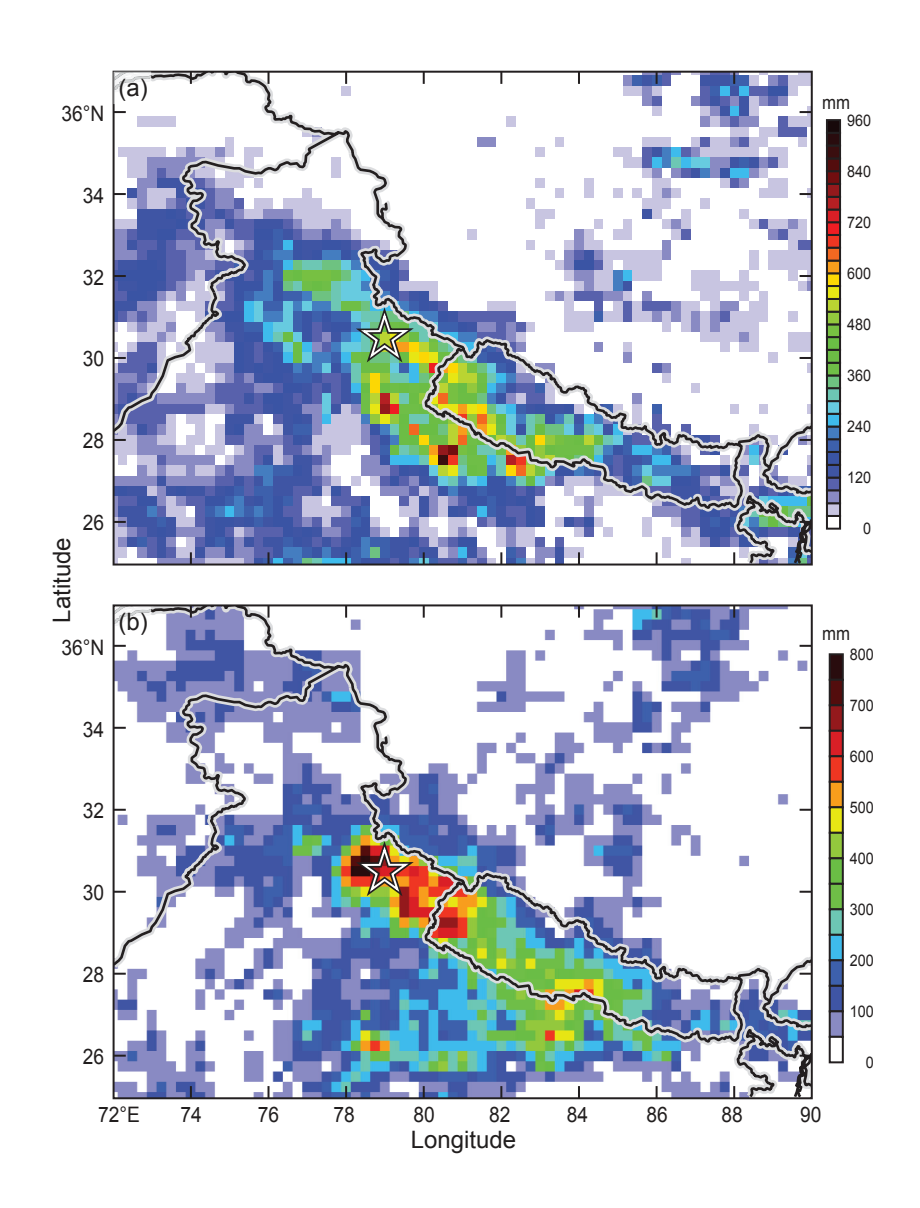
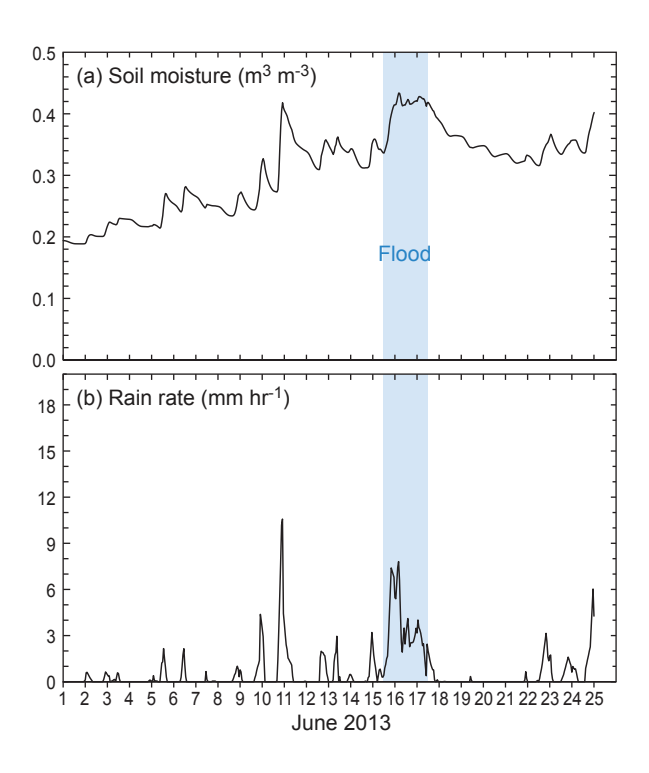


Figure 3. Meteosat-7 infrared satellite imagery for (a) 0000 UTC 11 June and (b) 0700 17 June 2013.



**Figure 4.** Accumulated rainfall over Uttarakhand from TRMM 3B42 for the periods (a) 7-13 June 2013 and (b) 14-17 June 2013.



**Figure 5.** NASA Goddard Land Information System (LIS) output with 3 km spatial resolution over the Uttarakhand region for month of June 2013. (a) Average rainfall rate in mm h<sup>-1</sup> (b) Average soil moisture (m³ of water per m³ of soil). Stations in the average are: Joshimath (30.56N, 79.57E), Uttarkashi (30.72N, 78.43E), Kedarnath (30.73N, 79.06E), and Almora (29.81N, 79.29E). See Figure 1b for locations.

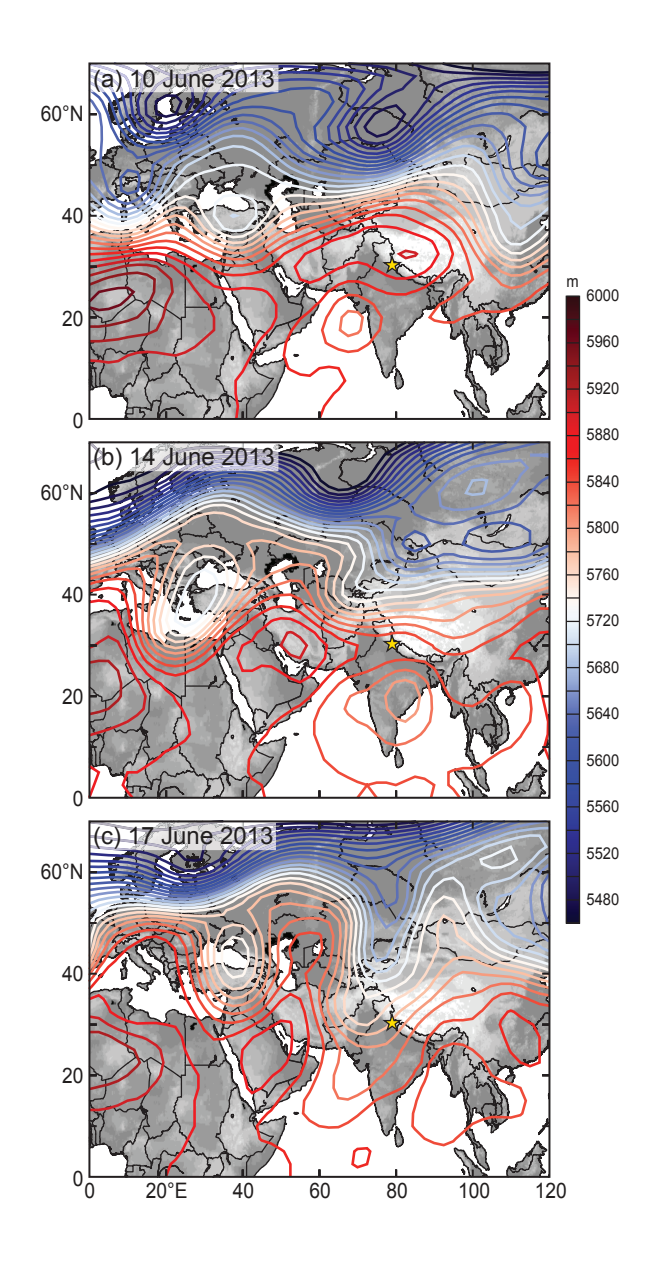
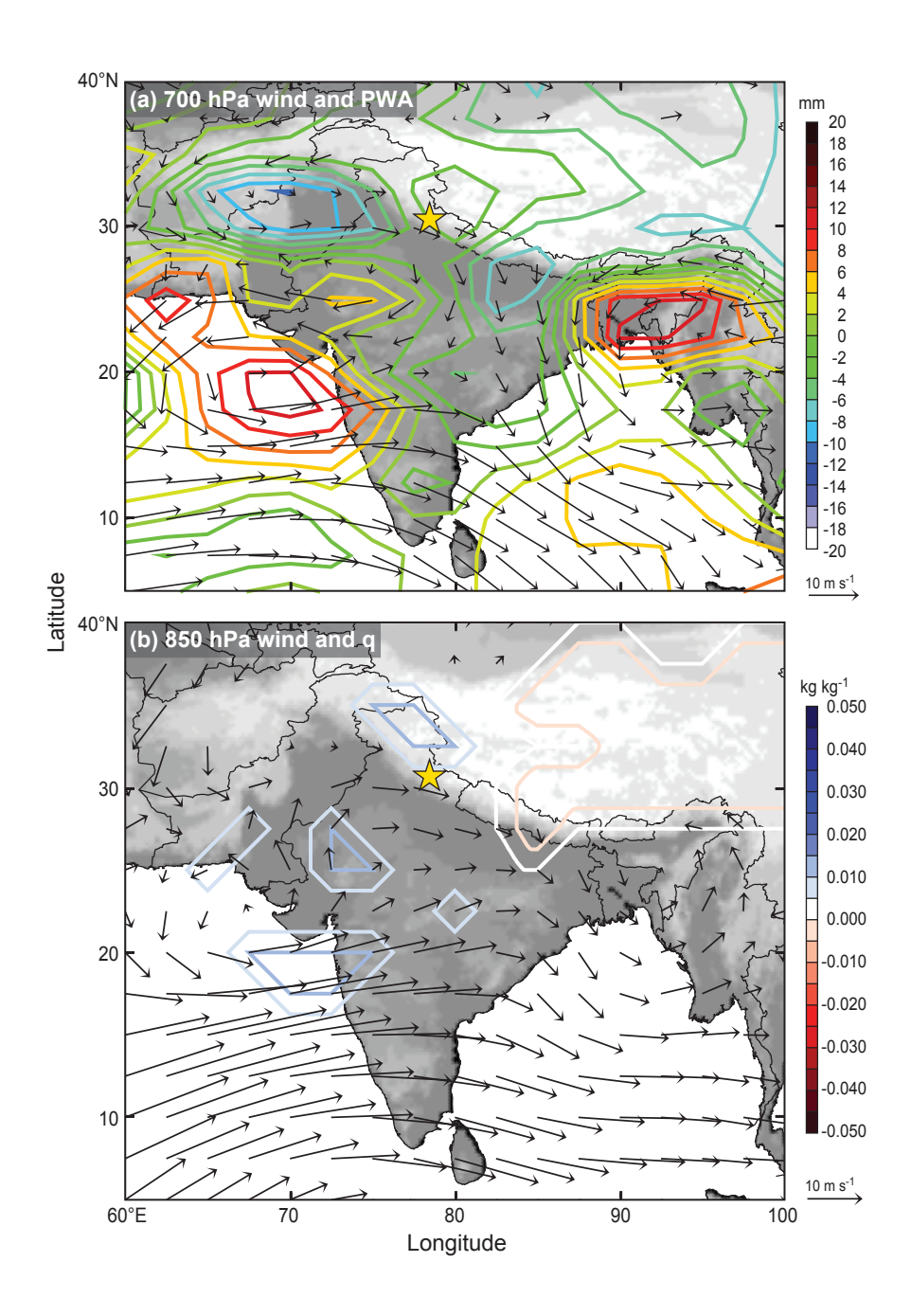


Figure 6. 500 hPa geopotential height (m) for (a) 10 June 2013, (b) 14 June 2013 and (c) 17 June 2013.



**Figure 7.** 10 June 2013 (a) mean precipitable water anomaly (mm) and 700 hPa wind, and (b) mean specific humidity anomaly (kg kg<sup>-1</sup>) and 850 hPa wind. Anomalies are departures from the monsoon seasonal mean (June-September).

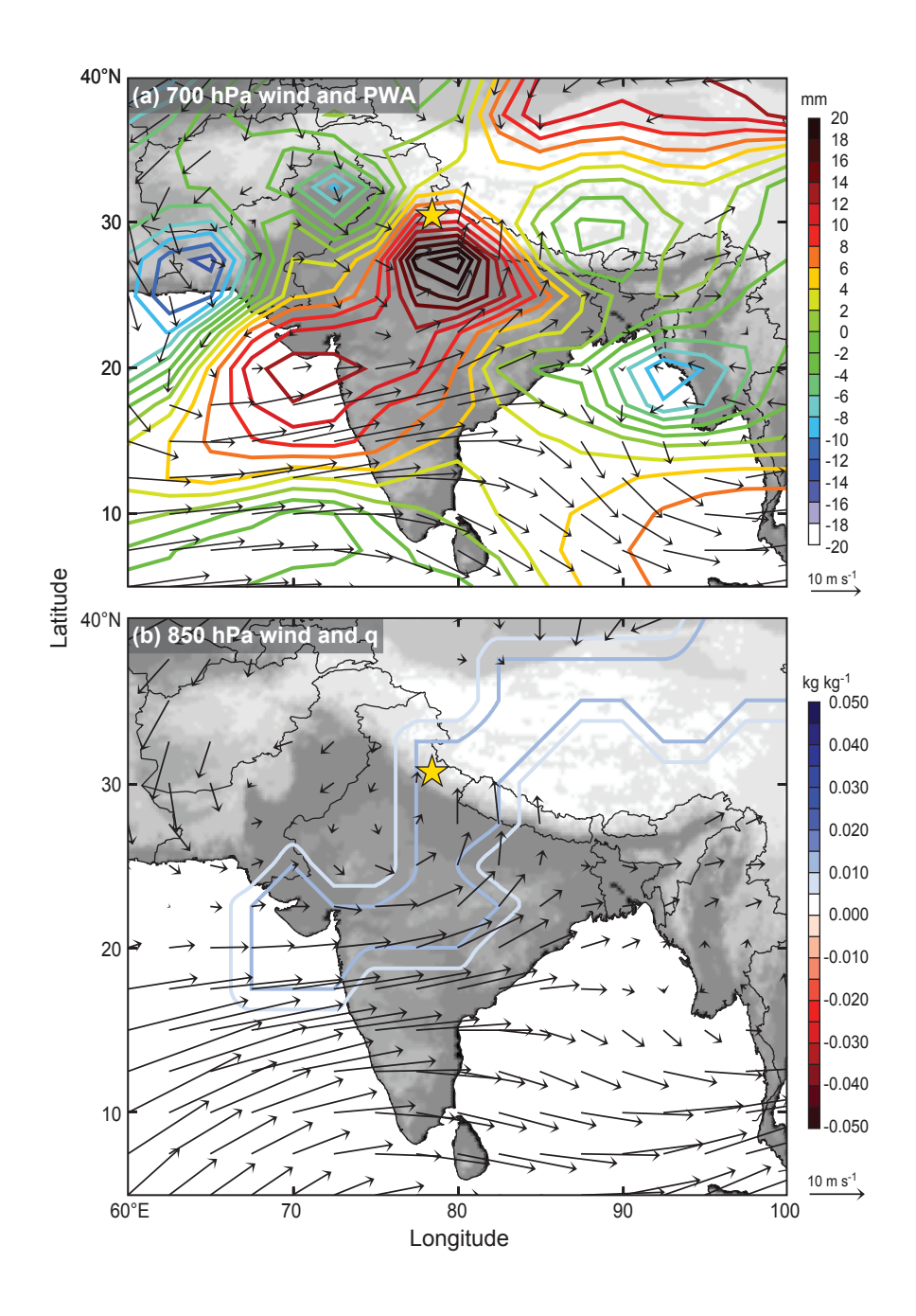
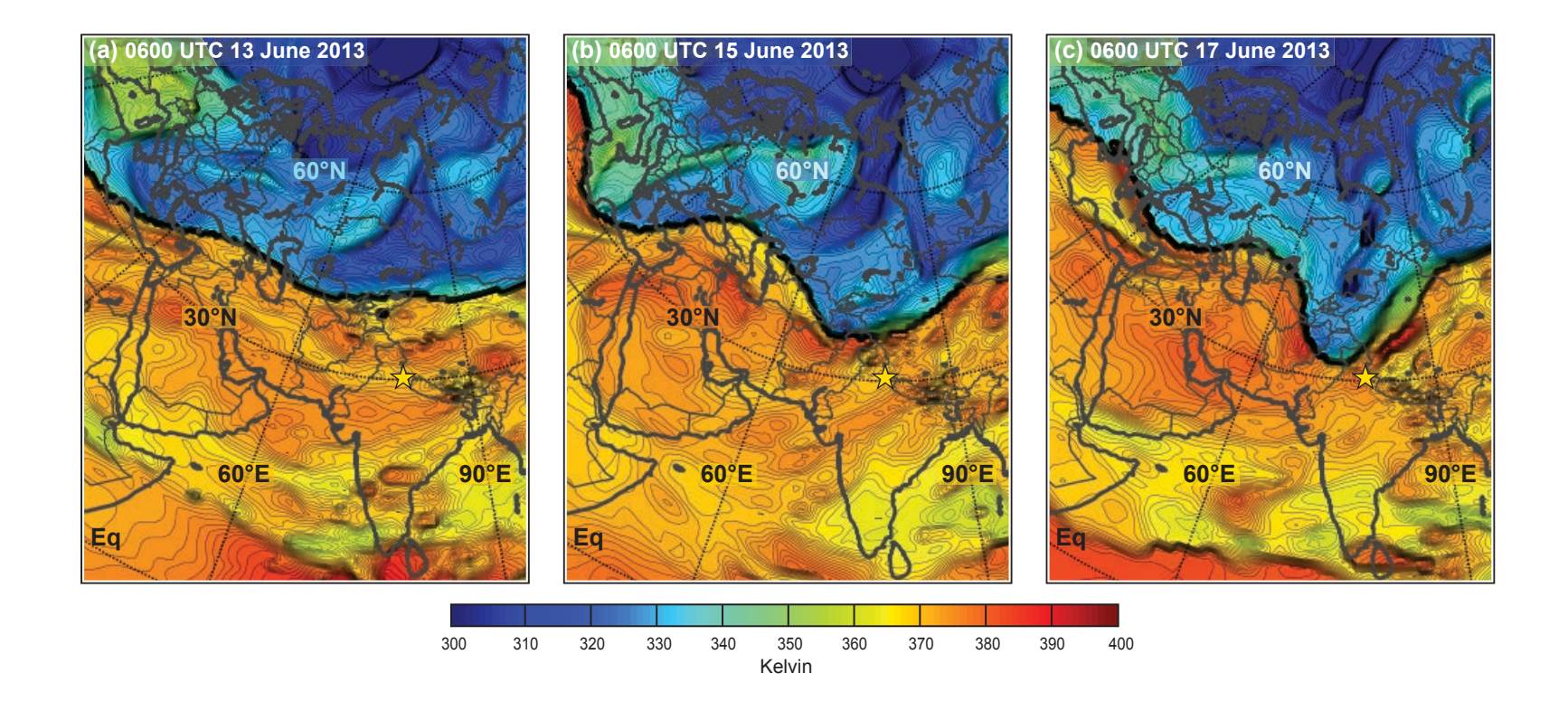
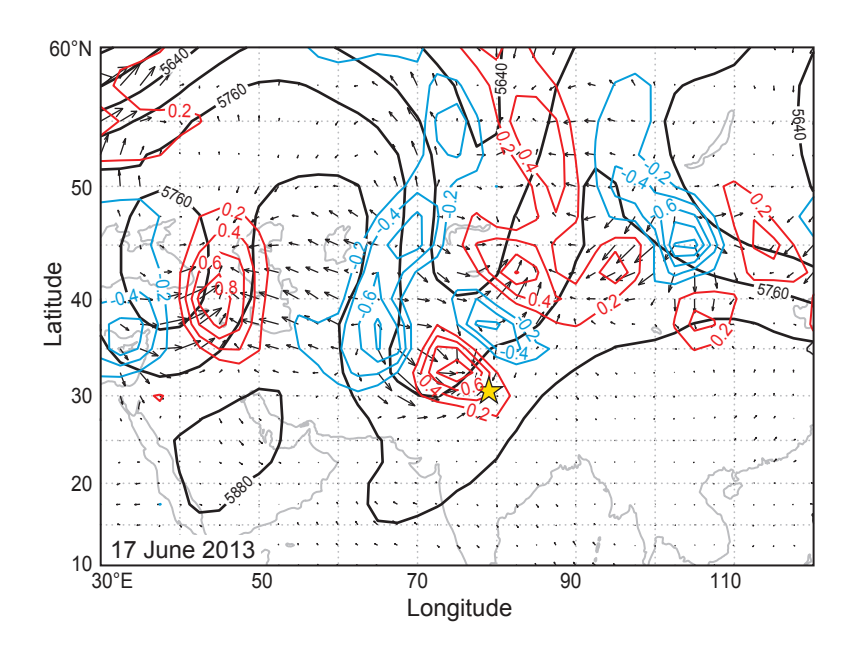


Figure 8. As in Figure 7 but for 17 June 2013.



**Figure 9.** (a)-(c) Sequence of ERA-interim 2 PVU (tropopause) plots of potential temperature  $(\theta)$ . Landmasses are outlined with heavy black borders. The dark line separating blue and orange shades occurs where the potential temperature lines are tightly packed and as such indicate the jet stream. The star shows the approximate location of the Uttarakhand flood.



**Figure 10.** 500 hPa heights in meters (black contours) for 17 June 2013 from NCEP/NCAR reanalysis. Calculated Q-Vectors are shown in black vectors. Regions of Q-Vector convergence (red contours), and Q-Vector divergence (blue contours) indicate synoptic-scale areas of rising (sinking) motion. The red and blue contours have units of 10<sup>17</sup> m kg<sup>-1</sup> s<sup>-1</sup>. The star shows the location of the Uttarakhand flood.

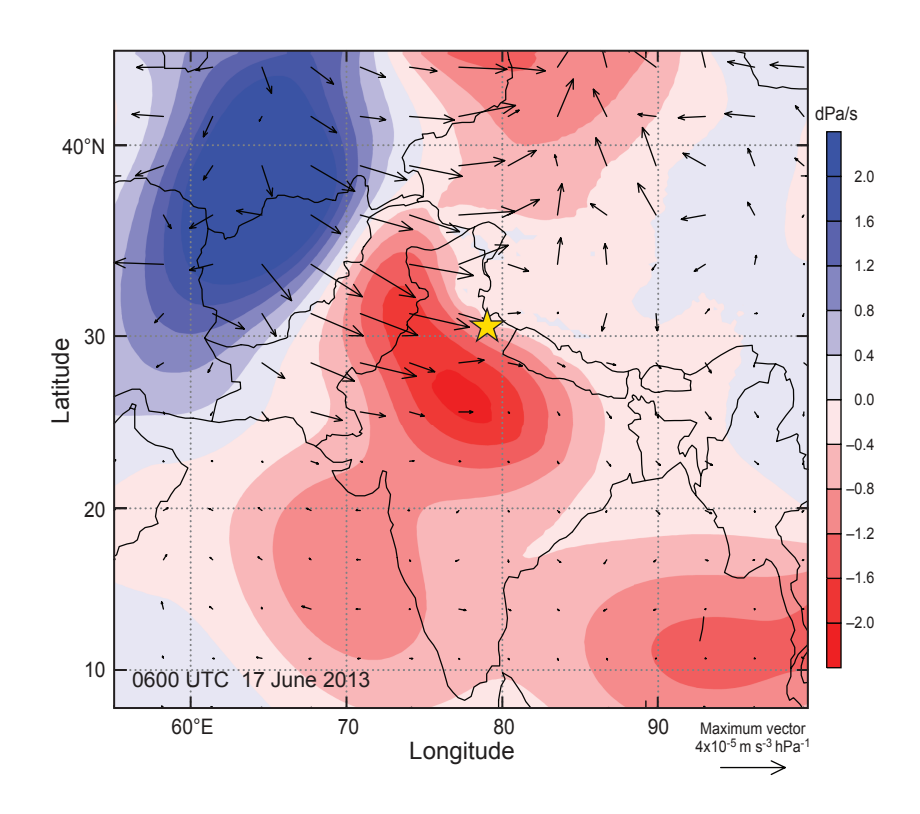


**Figure 11.** WRF model 500 hPa Q-vectors (black vectors). Upward motion (dPa s<sup>-1</sup>) implied by Q-vector convergence is in red shading. Downward motion implied by Q-vector divergence is in blue shading. The fields shown are for 0600 UTC 17 June 2013. The location of the Uttarakhand flood is denoted by the star.

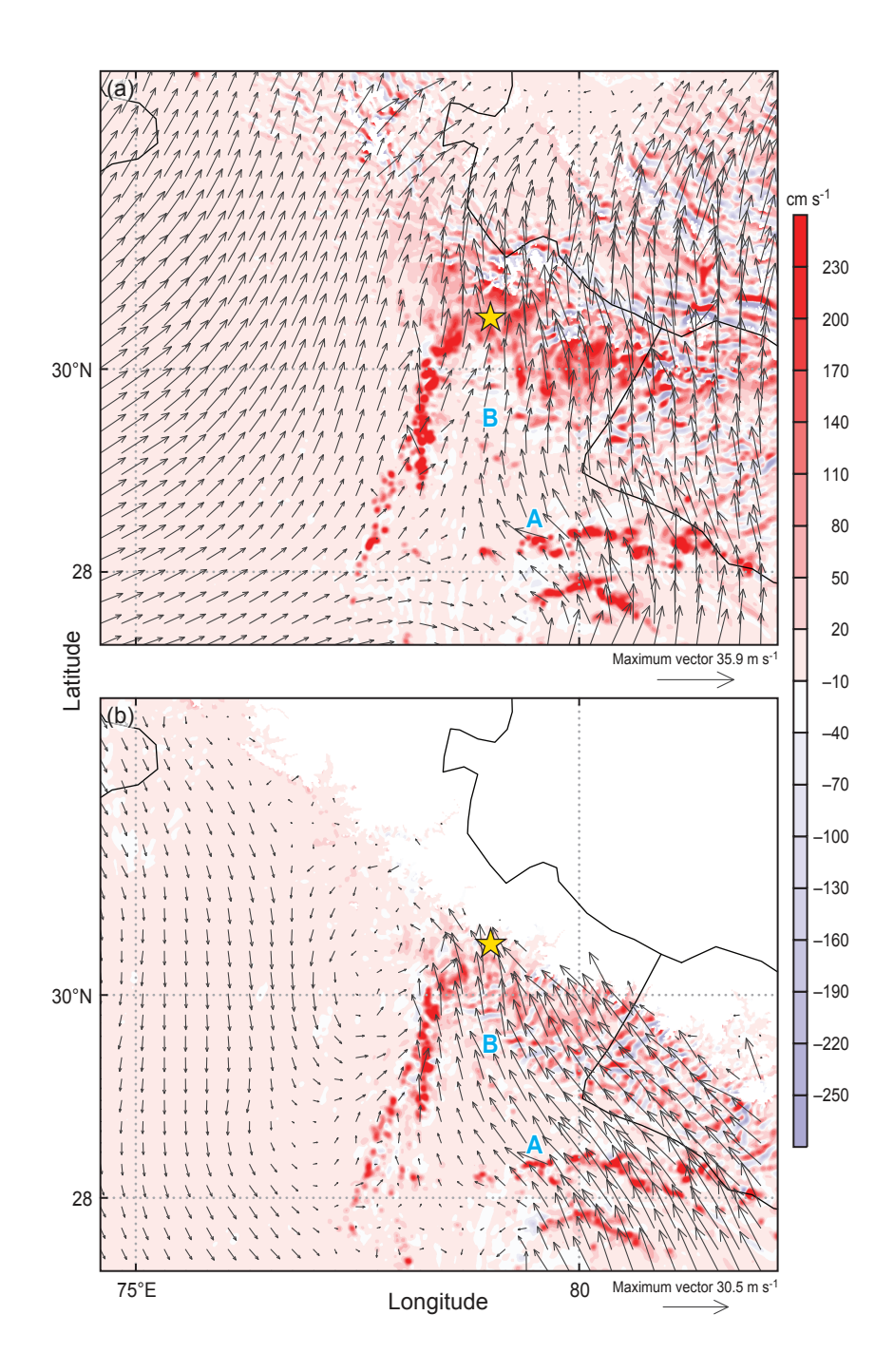


**Figure 12.** WRF simulation of vertical velocities (cm s<sup>-1</sup>)and horizontal winds (black vectors) for 0600 UTC 17 June 2013 for (a) 500 hPa, (b) 700 hPa. Red (blue) shading denotes upward (downward) vertical velocities. The points A and B indicate the locations of soundings shown in Figure 13.

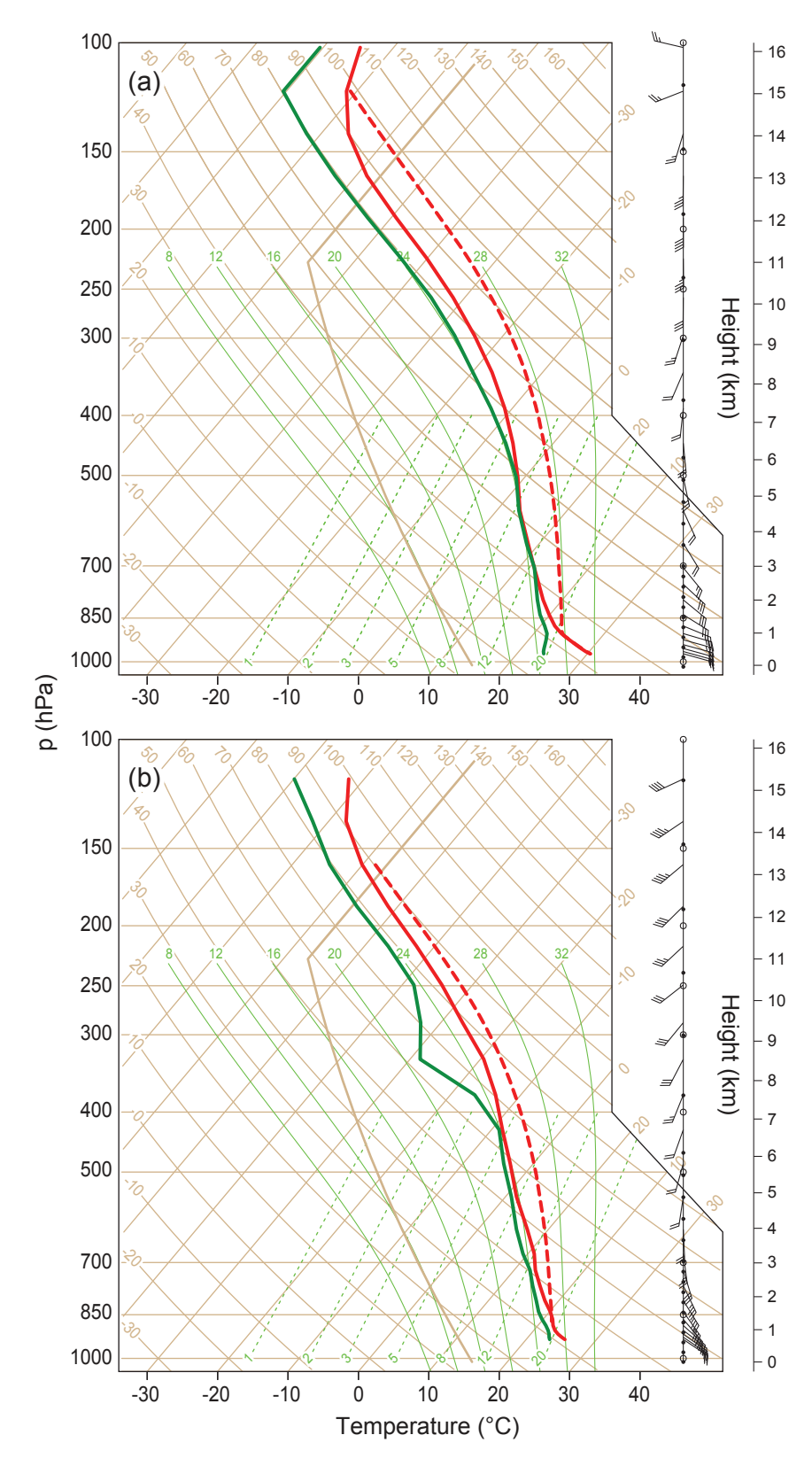


**Figure 13.** Soundings derived from WRF output for 0600 UTC 17 June 2013 for (a) point A and (b) point B in Figure MODELW. Temperature and dew point are displayed in Skew-T/Log-p format. The dashed red curves show the temperature of an undiluted parcel lifted from the surface.

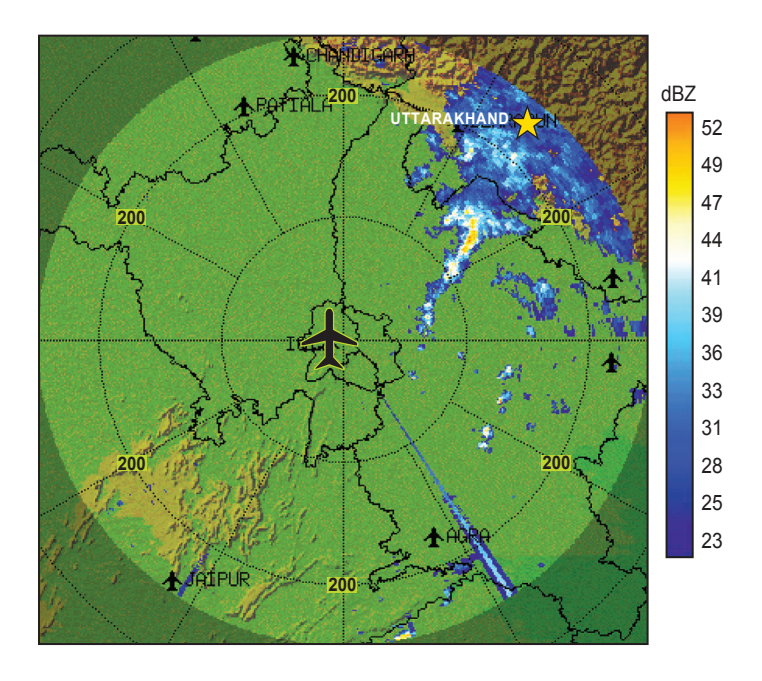


**Figure 14.** Low-level radar reflectivity (dBz) display from the operational radar at New Delhi Indira Gandhi International Airport (denoted by the airplane icon) at 0743 UTC 17 June 2013, during the Uttarakhand flood event. The color bar and image were available on the Indian Meteorological Department website. The star denotes the location of the Uttarakhand flood.

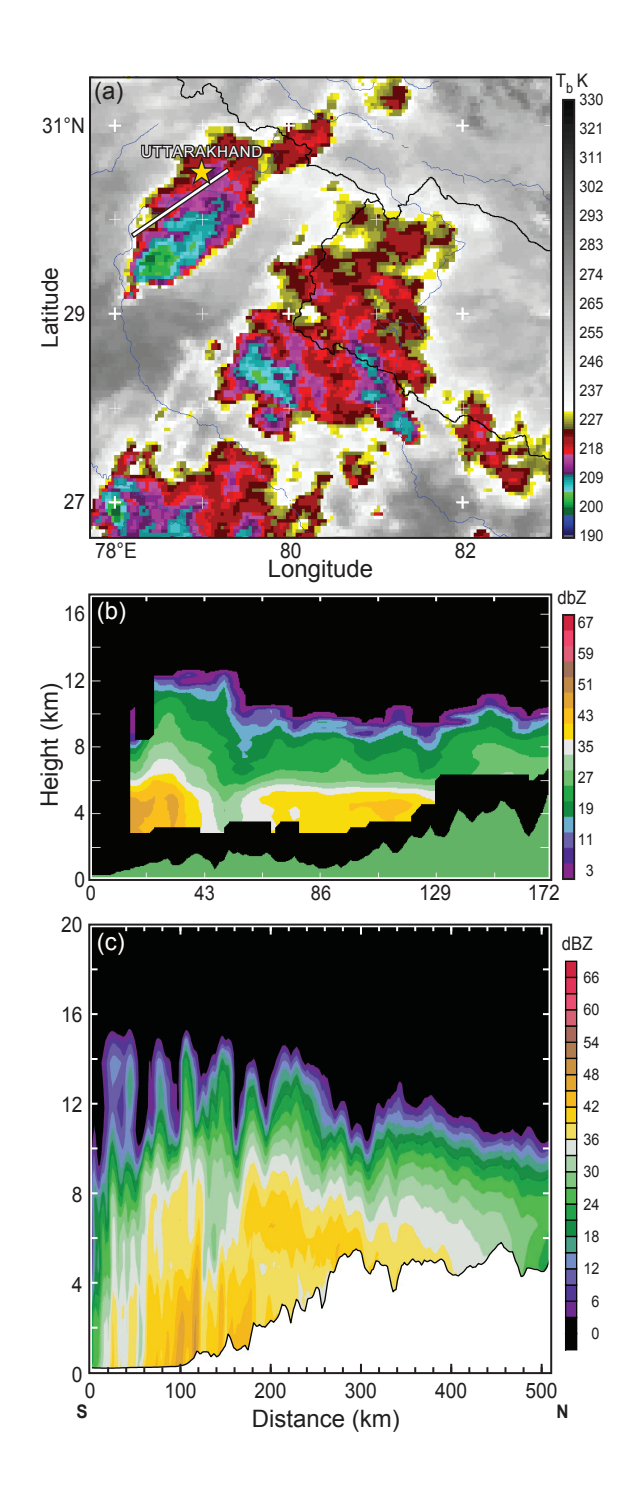


**Figure 15.** (a) *Meteosat-7* satellite infrared brightness temperatures (K). Star denotes location of flooding. (b) Vertical cross-section of TRMM PR data in dBZ taken left to right along the white line in (a). (c) WRF Radar reflectivity (d03) computed along a similar cross section to Figure 15b (Figure 2a) at 0700 UTC 17 June 2013.

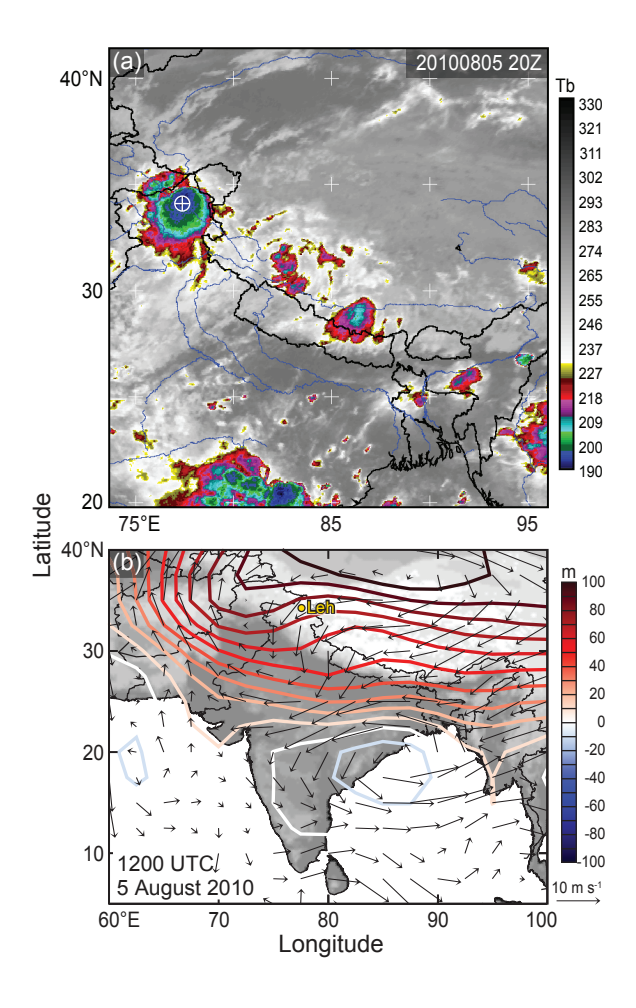


**Figure 16.** (a) *Meteosat-7* satellite infrared image (K) for 2000 UTC 5 August 2010 from *Meteosat-7* showing the MCS that resulted in the Leh flood. The location of Leh is indicated by a circled cross. (b) 500 hPa winds at 1200 UTC 5 August 2010. Contours show the 500 hPa height deviation from the seasonal average. Adapted from Rasmussen and Houze (2012).